International Journal of Hematology (2016.10) 104(4):491-501.

Iron-induced epigenetic abnormalities of mouse bone marrow through aberrant activation of aconitase and isocitrate dehydrogenase.

Masayo Yamamoto, Hiroki Tanaka, Yasumichi Toki, Mayumi Hatayama, Satoshi Ito, Lynda Addo, Motohiro Shindo, Katsunori Sasaki, Katsuya Ikuta, Takaaki Ohtake, Mikihiro Fujiya, Yoshihiro Torimoto, Yutaka Kohgo

Iron-induced epigenetic abnormalities of mouse bone marrow through aberrant activation of aconitase and isocitrate dehydrogenase

Masayo Yamamoto[1)], Hiroki Tanaka[2, 3)*], Yasumichi Toki[1)], Mayumi Hatayama[1)], Satoshi Ito[1)], Lynda Addo[1)], Motohiro Shindo[1)], Katsunori Sasaki[2)], Katsuya Ikuta[1)], Takaaki Ohtake[4)], Mikihiro Fujiya[1)], Yoshihiro Torimoto[5)], Yutaka Kohgo[4)]

1. Division of Gastroenterology & Hematology/Oncology, Asahikawa Medical University, Asahikawa, Hokkaido, Japan
2. Department of Gastrointestinal Immunology and Regenerative Medicine, Asahikawa Medical University, Asahikawa, Hokkaido, Japan
3. Department of Legal Medicine, Asahikawa Medical University, Asahikawa, Hokkaido, Japan
4. International University of Health and Welfare Hospital, Nasu-shiobara, Tochigi, Japan
5. Oncology Center, Asahikawa Medical University Hospital, Asahikawa, Hokkaido, Japan

Running title: Epigenetic and metabolic abnormalities by iron-overload

*Corresponding author

Hiroki Tanaka

Department of Gastrointestinal Immunology and Regenerative Medicine, Asahikawa Medical University, 2-1-1-1 Midorigaoka-Higashi. Asahikawa, Hokkaido 078-8510, Japan.

TEL +81-166-68-2462

FAX +81-166-68-2469

E-mail: hiroki-t@asahikawa-med.ac.jp

Abstract

Iron overload remains a concern in myelodysplastic syndrome (MDS) patients. Iron chelation therapy (ICT) thus plays an integral role in the management of these patients. Moreover, ICT has been shown to prolong leukemia-free survival in MDS patients; however, the mechanisms responsible for this effect are unclear. Iron is a key molecule for regulating cytosolic aconitase 1 (ACO1). Additionally, the mutation of isocitrate dehydrogenase (IDH), the enzyme downstream of ACO1 in the TCA cycle, is associated with epigenetic abnormalities secondary to 2-hydroxyglutarate (2-HG) and DNA methylation. However, epigenetic abnormalities observed in many MDS patients occur without IDH mutation. We hypothesized that iron itself activates the ACO1-IDH pathway, which may increase 2-HG and DNA methylation, and eventually contribute to leukemogenesis without IDH mutation. Using whole RNA sequencing of bone marrow cells in iron-overloaded mice, we observed that the enzymes, phosphoglucomutase 1, glycogen debranching enzyme, and isocitrate dehydrogenase 1 (Idh1), which are involved in glycogen and glucose metabolism, were increased. Digital PCR further showed that Idh1 and Aco1, enzymes involved in the TCA cycle, were also elevated. Additionally, enzymatic activities of TCA cycle and methylated DNA were increased. Iron chelation reversed these phenomena. In conclusion, iron activation of glucose metabolism causes an increase of 2-HG and DNA methylation.

Introduction

Myelodysplastic syndrome (MDS) is an acquired hematopoietic disorder caused by abnormalities in bone marrow stem cells and ineffective erythropoiesis, and is associated with a risk of transformation to acute leukemia [1, 2]. MDS patients suffer from chronic anemia and repeated red blood cell transfusions are required to sustain life. However, these transfusions may cause secondary iron overload, which eventually threatens their life due to liver dysfunction, heart failure, and infection [3].

Currently, iron chelation therapy (ICT) is performed worldwide to prolong the prognosis of MDS patients who undergo repeated blood transfusions [4, 5]. In addition, ICT could prolong leukemia free survival (LFS) in patients with MDS [6]. Therefore, ICT may prevent the conversion of MDS to acute leukemia and prolong the prognosis of MDS. Furthermore, some patients with MDS and/or acute leukemia receive a favorable, or sometimes a complete, clinical response only by ICT; [7-11] however, there are only a few such reported cases and it is not yet clear why ICT shows an anti-tumor effect.

In recent years, it was reported that the gene mutation of isocitrate dehydrogenase (*IDH*), the enzyme involved in the TCA cycle that converts isocitrate to α-ketoglutarate (α-KG), is associated with the development of certain gliomas [12, 13] and acute leukemias [14-18]. The gene product of mutated *IDH* forms a heterodimer with the wild-type IDH and changes the substrate binding site of IDH, which increases levels of 2-hydroxyglutarate (2-HG) with a concomitant decrease of α-KG [19]. α-KG acts as a substrate of the TCA cycle, whereas it is utilized in many other reactions including DNA demethylation [20-21]. Recently, *IDH* mutation and the up-regulation of DNA methylation were also predicted to be independent prognosis factors in patients with MDS [22-27]. Therefore, the mechanism of aberrant DNA methylation in patients with MDS is to be elucidated further.

Isocitrate, a substrate of IDH, is supplied from citrate by both cytosolic aconitase/iron responsive protein 1 (ACO1/IRP1) and mitochondrial aconitase (ACO2). In the cytosol, IDH1 which is a cytosolic isoform of IDH produces and supplies α-KG into mitochondria. ACO1/IRP1 has different roles depending on the cellular iron state. During an iron deficient status, it acts as IRP1, which combines with an iron responsive element (IRE) that exists on the untranslated region of the ferritin and transferrin receptor mRNA and regulates the expression of genes associated with iron regulation [28]. However, during an iron overloaded state, the [4Fe-4S]-cluster combines with the central region of protein activity and acts as ACO1 to

convert citrate to isocitrate in the TCA cycle [28, 29]. In turn, iron overload in the human erythroleukemia cell line K562 changes the expression and activity of enzymes involved in the TCA cycle (i.e., IDH and ACO1) [30]. Therefore, it seems that iron overload has an impact on enzymes involved in glucose metabolism.

From these reports, we hypothesized that iron overload itself in bone marrow cells may induce epigenetic abnormalities through the expression and activity of enzymes involved in cellular metabolism, particularly in the TCA cycle, which may eventually affect DNA methylation and exacerbate MDS and/or the progression of MDS to leukemia. In the present study, we performed whole RNA sequencing in iron overloaded mouse bone marrow cells to evaluate changes in gene expression, especially those associated with cellular metabolism, and changes in 2-HG production and DNA methylation by iron. Furthermore, we examined how iron chelation affected DNA methylation in an iron overloaded state.

Materials and methods

Animals

Male C57BL/6 mice (Clea Japan, Tokyo, Japan) were randomly assigned into following 3 separate treatment groups at age 8 weeks, Control: PBS (100 μL/head/day) was injected, Fe: iron dextran (10 mg/head/day) (Sigma-Aldrich, St. Louis, MO, USA) was injected, Fe + DFO: once iron dextran (10 mg/head/day) was injected, then 6 hours later, deferoxamine (DFO: 100 mg/kg/day) (Abcam, Cambridge, England) was injected. These injections were intraperitoneally performed for 5 days. The mice were sacrificed at the 6th day, and then bone marrow cells were collected from thighbones. Bone marrow smears were processed for Prussian blue staining. All animal experiments were approved by the Animal Experiments Committee of the Asahikawa Medical University (Hokkaido, Japan) based on the guidelines for animals protection.

Measurements of intracellular iron level in bone marrow

Bone marrow cells were lysed in 0.1 N nitric acid, and intracellular iron levels were measured by an atomic absorption analysis system (Hitachi Z-8100, Tokyo, Japan). The iron standard solution 100 mg/L (Wako, Osaka, Japan) was used as a standard.

Whole RNA sequencing

RNA was extracted from bone marrow cells using the PureLink RNA Mini Kit (Life Technologies, Carlsbad, CA, USA). Ribosomal RNA was then eliminated using the RiboMinus Eukaryote System (Life Technologies). The RNA was reverse transcribed to obtain cDNA library using the Ion Total RNA-Seq Kit (Life Technologies), and a sequence reaction was performed using the high throughput sequencer Ion Proton (Life Technologies). Whole RNA sequencing analysis was performed using the CLC bio Genomic Workbench (CLC bio, Aarhus, Denmark), and the reads per kilobase of exon model per million mapped reads (RPKM) was measured as gene expression levels.

Digital PCR analysis

cDNA was reverse transcribed from RNA extracted from the bone marrow cells using the high capacity cDNA Reverse Transcription Kit (Life Technologies). The copy numbers of mouse *Aco1*, isocitrate dehydrogenase 1 (*Idh1*), phosphoglucomutase 1 (*Pgm1*), and glycogen debranching enzyme (*Agl*) mRNA were then analyzed using a digital PCR system (QuantStudio 3D Digital PCR system, Life Technologies) with the TaqMan probe for mouse *Aco1*, *Idh1*, *Pgm1*, and *Agl* (Life Technologies).

Measurements of enzyme activity

Intracellular aconitase activity was measured using an Aconitase Assay Kit (Abcam), whereas intracellular IDH activity was measured using an Isocitrate Dehydrogenase Activity Colorimetric Assay Kit (BioVision, Mountain View, CA, USA). A multimode plate reader EnsPire (PerkinElmer, Waltham, MA, USA) was used for the analysis.

Analysis of intracellular metabolite production

Bone marrow cells were lysed in 0.1 N hydrochloric acid. Afterwards, whole organic acids in each sample were extracted by salting-out methods. Briefly, sodium chloride and ethyl acetate were added into the lysates. After centrifugation, the ethylacetate phase was collected. Finally, trimethylsilylating agents (Sigma-Aldrich) were added into the samples, and intracellular metabolite production was measured by gas chromatography mass spectrometry (GC-MS) using JMS-T100GCV (JEOL, Tokyo, Japan).

Quantification of DNA methylation

DNA was extracted from bone marrow cells using the DNeasy Blood & Tissue Kit (QIAGEN, Tokyo, Japan). The ratio of methylated cytosine to whole DNA was analyzed by Enzyme-Linked ImmunoSorbent Assay (ELISA) using the MethylFlash Methylated DNA Quantification Kit (Epigentek, Farmingdale, NY, USA). A multimode plate reader EnsPire (PerkinElmer) was used for the measurement.

Statistics

The Student's parried t-test was used. A *P*-value <0.05 was considered statistically significant.

Results

Change of iron status in bone marrow cells

We evaluated the changes in the iron status of bone marrow cells in the iron overloaded and chelated mice. According to the Prussian blue staining of bone marrow cells, the iron overloaded mice showed significantly stronger iron deposits than the control mice; however, iron chelated mice showed reduced iron deposits compared to iron overloaded mice (Figure 1A). Intracellular iron levels in the bone marrow were significantly higher in iron overloaded mice than the control group. However, the intracellular iron levels were significantly lower in iron chelated mice than the iron overloaded mice (Figure 1B). In our preliminary experiments, iron deposits were even observed 6 hours later of single iron injection (data not shown). We have previously reported that the serum Non-transferrin bound iron (NTBI) was up-regulated in same mouse model [31]. It has not been clarified how the NTBI go into the cell until now. However, it is considered that NTBI go through the cell membrane more than transferrin bound iron. Therefore, iron overload by iron dextran treatment and iron chelation by DFO was sufficient and effective, respectively, in this mouse model.

Whole RNA sequencing analysis in bone marrow

After iron loading and chelation, whole RNA sequencing analysis was performed to evaluate any changes in gene expression in the mice bone marrow cells in the iron overload (n = 2), iron chelation (n = 2), and control (n = 2) groups. In total, the levels of 38124 mouse gene transcripts were analyzed. We then compared the gene expression changes of the control group versus the iron overload group and the iron overload group versus the iron chelation group. Of the 38124 gene transcripts, we focused on those whose absolute fold changes were >1.5, and observed changes in the expression levels of 9311 genes (6113 up-regulated and 3198 down-regulated genes) when we compared the control and iron overload groups (Figure 2-A, pink and green areas). However, when the iron overload and iron chelation groups were compared (Figure 2-B, pink and green areas), changes in the expression levels of 11043 genes (5782 up-regulated and 5261 down-regulated genes) were observed. We then extracted those genes whose changes in expression were found to be significant (*P*-value <0.05). As a result, 101 genes (46 up-regulated and 55 down-regulated genes) and 256 genes (81 up-regulated and 175 down-regulated genes) were extracted from the comparison between the control and iron overload groups (Figure 2-A, pink area) and the iron overload and iron chelation groups (Figure 2-B, pink area), respectively. We then focused on 22 genes whose expression were observed to overlap with the 2 comparison groups (Figure 2-C and Table 1). Regarding the functions of these 22 gene products, 4 genes were directly associated with glycogen and glucose metabolism. These genes were Pgm1 and Agl, which are associated with glycogenolysis, and Idh1 and Idh3a, which are associated with the TCA cycle (Table 1). All these genes were found to be increased in the iron overloaded state, but decreased after iron chelation. All 4 genes have specified roles in glucose metabolism, and therefore, we hypothesized that the genetic expression of enzymes involved in glucose metabolism were most likely affected by iron overload in the bone marrow.

Gene expression changes associated with glucose metabolism

The mRNA of *Pgm1* and *Agl* codes enzymes which produce glucose from glycogen, and the mRNA of *Idh1* codes the rate-limiting enzyme of the TCA cycle. These gene expressions were significantly impacted by iron overload and chelation in bone marrow as a result of whole RNA sequencing analysis. Additionally, cytosolic aconitase (ACO1), which produces and supplies isocitrate to IDH in the TCA cycle, was also known to be activated by iron overload. Therefore, we tried to validate the changes in gene expression in these 4 genes by digital PCR analysis. The expressions of *Aco1* and Idh1 were increased in the iron overloaded mice compared to

controls, but significantly decreased in the iron chelated mice compared to iron overloaded mice (Figure 3). *Pgm1* expression was slightly increased in the iron overloaded mice compared to controls, but no significant change was observed between the iron chelated and overloaded mice (Figure 3). *Agl* expression was significantly increased in the iron overloaded mice compared to controls, but no significant change was observed between the iron chelated and overloaded mice (Figure 3). Because the sensitivity of RNA sequencing analysis was lower than that of digital PCR analysis, the discrepancies were observed in the results of these two analysis. According to these results, *Aco1* and *Idh1*, which are associated with the TCA cycle, were particularly affected by iron overload during glucose metabolism.

Enzyme activity changes of aconitase and isocitrate dehydrogenase

We then investigated how the changes in the mRNA expression of *Aco1* and *Idh1* by iron overload affect enzymatic activities. The mice bone marrow cells were lysed in optimized buffer for each assay. The intracellular activity of ACO and IDH were then enumerated by colorimetric assay. The bone marrow enzyme activities of both ACO and IDH were increased in the iron overloaded mice compared to controls, but significantly decreased in the iron chelated mice compared to those in the iron overloaded state (Figure 4). Therefore, iron overload in the bone marrow enhanced the enzymatic activities of both ACO and IDH, and these phenomena were reversed by iron chelation.

Changes in the production of metabolites in the TCA cycle

The activations of ACO and IDH enzyme activity suggested an over-production of intermediate metabolites in the TCA cycle. In addition, an imbalanced TCA cycle caused by gene mutations in enzymes such as *IDH*, succinate dehydrogenase (*SDH*), and fumarate hydratase (*FH*), has been reported to cause an accumulation of the aberrant metabolite 2-HG [31, 32]. We then evaluated the intracellular levels of α-KG and 2-HG, which are intermediate metabolites produced by ACO1-IDH activity in the TCA cycle, in the bone marrow lysates using GC-MS analysis. The total level of intracellular α-KG was increased in the iron overloaded mice compared to controls, but significantly decreased in the iron chelated mice compared to iron overloaded mice (Figure 5). Furthermore, the total intracellular 2-HG level was also increased in the iron overloaded mice compared to controls, but significantly decreased

in the iron chelated mice compared to those in the iron overloaded state (Figure 5). According to these findings, the supply of substrates in the enzymatic reaction of IDH and the activity of IDH itself were significantly up-regulated by iron.

Changes in DNA methylation by iron overload

It has been reported that an over-production of 2-HG caused by the *IDH* mutation induces hypermethylation of DNA and promotes carcinogenesis [14-20]. Therefore, we suspected that the over-production of 2-HG, which was induced by iron overload, resulted in hypermethylation of DNA even in the absence of an *IDH* mutation. Afterwards, we evaluated DNA methylation levels in the bone marrow by ELISA utilizing anti-methylcytosine specific antibody. We observed that the percentages of DNA methylation were increased in the iron overloaded mice compared to controls, but significantly decreased in the iron chelated mice compared to iron overloaded mice (Figure 6). According to these results, iron overload activated the ACO1-IDH pathway, which resulted in an increase in the production of α-KG and 2-HG. The change in metabolite production correlated with each other; therefore, we hypothesized that increased 2-HG production in the iron overloaded state was a result of supplying isocitrate to IDH through the activation of ACO1 and increased activity of IDH, which resulted in an increase in DNA methylation even in the absence of an IDH mutation (Figure 7). Furthermore, these phenomena were reversible by iron chelation.

Discussion

In recent reports, it has been shown that ICT prolonged the leukemia free survival in MDS patients [6], and patients with MDS and/or acute leukemia had remission by only ICT [7-11]. Both of these findings suggest a link between iron and leukemogenesis. Concerning the mechanism, DNA methylation is considered to be associated with the pathogenesis and exacerbation of MDS [23-27]. In the present study, we first demonstrated that iron overload activated the ACO1-IDH pathway in the TCA cycle and led to increased 2-HG activity, which induced DNA methylation, a critical epigenetic aberration process. In the TCA cycle, ACO1 and IDH1, which are enzymes associated with glucose metabolism, were especially activated by iron overload. Furthermore, these phenomena were canceled by iron chelation.

As previously indicated, ACO1/IRP1 has 2 different roles depending on the metabolism of

iron. ACO1 is mainly present in an iron overloaded state, whereas IRP1 is present in the iron deficient state [28, 29]. Therefore, the activation of ACO1 seems to be increased by iron overload. IDH enzyme activity has also been reported to be activated by iron loading in human cell lines [30]. However, it was not clear whether the change of IDH activity resulted from ACO1 activation or from iron overload itself. Further studies are required to clarify these mechanisms.

Another issue to be resolved is how 2-HG was increased by iron overload and decreased by iron chelation in the present conditions. A typical explanation for the increase in 2-HG is the *IDH* gene mutation, which results in heterodimerization of IDH-mutated molecules and wild-type molecules [19]. Actually, the association between the mechanisms of carcinogenesis and 2-HG in glioma and acute leukemia were focused on the *IDH* mutation [12-18]. During *IDH* mutation conditions, the conversion from 2-HG to α-KG by 2-hydroxyglutarate dehydrogenase (2-HGDG) is not sufficient for the over-production of 2-HG, which results in an excess of 2-HG [34]. However, this was not a probable explanation for our current model of iron overload, because there were no IDH mutations in the C57BL/6 mice that were used for this study. The following explanations were predicted in order to understand the increment of 2-HG in a physiological condition without an *IDH* mutation: 2-HG was produced from α-KG by hydroxyacid oxoacid transhydrogenase (HOT) [35], and 2-HG was converted to α-KG by 2-HGDG [34]. In addition, we determined that 2-HG was increased in bone marrow cells without an *IDH* mutation through the activation of the ACO1-IDH pathway by iron overload in the present study. Therefore, we can hypothesize some mechanisms for the increase in 2-HG. Firstly, the activation of ACO1 and IDH increases the production of isocitrate and α-KG. It is also possible that the insufficient conversion of α-KG to succinyl-CoA causes an increase in α-KG levels, which can increase the production of 2-HG by HOT. In this regard, we confirmed the increase of α-KG by iron overload. Next, while NADP acted as a coenzyme in the conversion of isocitrate to α-KG [19], NADPH acted as a coenzyme for the conversion of α-KG to 2-HG [19]. The balance of NADP / NADPH plays an important role in 2-HG production. Therefore, it is possible that cellular iron overload disturbs the NADP / NADPH balance and causes an increase in 2-HG production. Finally, there was a possibility that the activity of 2-HGDG was decreased by iron overload, which can inhibit the conversion of 2-HG to α-KG. Further studies are necessary to describe the mechanisms that contribute to the increase in 2-HG levels.

The differences in the increase of 2-HG levels between the *IDH* mutation models and our

iron overloaded model need to be further clarified. While it was reported that 2-HG was increased 10- to 100-fold in patients with an *IDH* mutation [14-16, 36-41], 2-HG was only increased 2-fold in the iron overloaded mice compared to the control group in the present study. From these results, we considered that DNA methylation accumulated by the long-term exposure of 2-HG in bone marrow cells was associated with leukemogenesis even during small increase in the levels of 2-HG compared to cases with an *IDH* mutation.

In this study, we demonstrated that iron overload activates the ACO1-IDH pathway, increases 2-HG levels, and results in DNA hypermethylation. From our study, we hypothesized that iron overload resulted in the increase of 2-HG production and DNA methylation by the activation of ACO1-IDH pathway in patients with MDS or acute leukemia despite the presence or absence of an *IDH* mutation. Consequently, ICT for iron overload might decrease DNA methylation through the control of the ACO1-IDH pathway, and might be effective for patients with MDS or acute leukemia. In this regard, the extent to which DNA methylation was accelerated by iron overload was not clear. Furthermore, it was not clear whether the increase of 2-HG and DNA methylation resulted from iron overload in patients without an IDH mutation. Additional studies are needed to clarify these issues.

Furthermore, the iron overloaded state is prolonged in MDS patients because of blood transfusions that lasted for a long time; however, a short-term model for iron overload was used in the present study. Therefore, future studies should be conducted to compare long- and short-term iron overload mice models and specifically evaluate the amount of DNA methylation.

In conclusion, DNA methylation was increased by iron overload through the increase of 2-HG in mice without an *IDH* mutation; this effect was inhibited by iron chelation. Therefore, ICT in transfusion-induced iron overload prevent not only cellular iron toxicities but also epigenetic tumorigenesis through the intervention to DNA hypermethylation by iron.

Authorship and Disclosures

YT, MH, SI and LA participated in making iron-overload mice; MY and HT performed all analysis in this work; KS, KI, TO, MF and YT gave helpful suggestions to conduct all analysis; MY, HT and YK wrote the manuscript. This work was supported in part by a Grant-in-Aid for Scientific Research <KAKENHI> and Health and Labor Sciences Research Grant. The Department of Clinical Gastroenterology is endowed by Kyorin Phamaceutical Co., Ltd. (Tokyo,

Japan), Sapporo Higashi Tokushukai Hospital (Sapporo, Japan), Asahi Kasei Medical Co., Ltd. (Tokyo, Japan), and Novartis Pharmaceuticals Japan Co., Ltd. (Tokyo, Japan). All of our projects involving iron metabolism are performed in collaboration with Novartis Pharmaceuticals Japan Co., Ltd. and Chugai Pharmaceuticals Japan Co., Ltd. (Tokyo, Japan). The authors would like to thank Mr. Hiroaki Akutsu (Center for Advanced Research and Education, Asahikawa Medical University, Hokkaido, Japan) for the technical assistance during GC-MS analysis. The original version of this manuscript have been published in Hokkaido Igakuzasshi (89 (2) : 125-131 , 2014) written in Japanese. Upon the official approval of Hokkaido Igakuzasshi, the English version of manuscript was re-submitted to this journal.

Table 1. Expression changes in the 22 extracted genes

Function	Gene name	Name of gene product	Cont. (means of RPKM)	Fe (means of RPKM)	DFO (means of RPKM)	FC (cont. vs Fe)	*P* value (cont. vs Fe)	FC (Fe vs DFO)	*P* value (Fe vs DFO)
Enzymes associated with glucose metabolism	*Pgm1*	Phosphoglucomutase 1	0.1003	0.2013	0.1032	2.0075	0.0040	-1.9508	0.0068
	Agl	Glycogen debranching enzyme	0.0121	0.0829	0.0315	6.8333	0.0010	-2.6324	0.0328
	Idh1	Isocitrate dehydrogenase 1	0.0881	0.4217	0.1030	4.7888	0.0350	-4.0934	0.0389
	Idh3a	Isocitrate dehydrogenase 3a	0.1179	0.3353	0.0442	2.8435	0.0380	-7.5868	0.0234
RNA polyadenilation enzyme	*Fip1l1*	Factor Interacting With PAPOLA And CPSF1	0.0402	0.0961	0.0260	2.3924	0.0480	-3.6883	0.0123
DNA repairing protein	*Fancm*	Fanconi Anemia, Complementation Group M	0.0303	0.1575	0.0521	5.2021	0.0170	-3.0222	0.0290
Regulation of lipogenesis	*Mid1ip1*	MID1 Interacting Protein 1	0.0913	0.2612	0.1712	2.8595	0.0020	-1.5262	0.0078
Extracellular matrix glycoprotein	*Lamc1*	Laminin, Gamma 1	0.0411	0.1563	0.1031	3.8053	0.0090	-1.5154	0.0127
Intracellular protein transport	*Heatr5b*	HEAT Repeat Containing 5B	0.0590	0.1419	0.0219	2.4063	0.0490	-6.4941	0.0335
Enzymes in the biosynthesis of coenzyme A	*Pank1*	Pantothenate Kinase 1	0.0000	0.1869	0.0000	∞	0.0114	-∞	0.0114
Aminoacyl-tRNA synthetases	*Gars*	Glycyl-TRNA Synthetase	0.1970	0.4190	0.0294	2.1267	0.0195	-14.2368	0.0192
Regulator of cytokinesis	*Kif20b*	Kinesin Family Member 20B	0.1457	0.2202	0.0126	1.5109	0.0369	-17.4127	0.0388
Golgi-derived retrograde transport vesicles with the ER	*Stx18*	Syntaxin 18	0.0000	0.0904	0.0000	∞	0.0464	-∞	0.0464
RNA gene with undefined RNA class	*SNORD121 A*	Small Nucleolar RNA, C/D Box 121A	0.0000	4.6787	0.0000	∞	0.0464	-∞	0.0464
G-protein binding and guanyl-nucleotide exchange factor	*Ric8b*	RIC8 Guanine Nucleotide Exchange Factor B	0.0000	0.1235	0.0000	∞	0.0464	-∞	0.0464
ABL1 and/or ABL2 binding protein	*Abi2*	Abl-Interactor 2	0.0000	0.0657	0.0000	∞	0.0464	-∞	0.0464
Member of the histone H4 family	*Hist1h4j*	Histone Cluster 1, H4j	2.3926	5.0486	1.9217	2.1101	0.0380	-2.6271	0.0132
RNA interference protein	*Ago4*	Argonaute RISC Catalytic Component 4	0.5240	0.0803	0.1409	-6.5222	0.0220	1.7535	0.0009
Protein sialylation	*St8sia4*	ST8 α-N-Acetyl-Neuraminide α-2,8-Sialyltransferase 4	0.0417	0.0225	0.0895	-1.8539	0.0410	3.9845	0.0138
Transcription factor for maturation of T cell	*Hlx*	H2.0-like homeobox protein	0.2525	0.1466	0.3329	-1.7222	0.0460	2.2707	0.0399
Endoplasmic reticulum transport	*Syt11*	synaptotagmin-like protein 1	0.2805	0.0414	0.3023	-6.7730	0.0200	7.2997	0.0039
Cell cycle checkpoint control	*Rint1*	RAD50 Interactor 1	0.1351	0.0223	0.1193	-6.0523	0.0190	5.3445	0.0349

Yellow: up-regulated by iron and down-regulated by iron chelation.

Green: down-regulated by iron and up-regulated by iron chelation.

RPKM, Reads per kilobase of exon model per million mapped reads; FC, Fold change

References

1. List A.F., Sandberg A.A., Doll D.C., Myelodysplastic Syndromes. In: Greer JP, Foerster J, Lukens J.N., Rodgers G.M., Paraskevas F., Glader B., editors. Wintrobe's Clinical Hematology. 11th ed. Philadlphia: Lippincott Williams & Wilkins; 2004. p. 2207-34.

2. Shlush LI, Zandi S, Itzkovitz S, Schuh AC, Aging, clonal hematopoiesis and preleukemia: not just bad luck? Int J Hematol. 2015;102:513-22

3. Takatoku M, Uchiyama T, Okamoto S, Kanakura Y, Sawada K, Tomonaga M, et al. Retrospective nationwide survey of Japanese patients with transfusion-dependent MDS and aplastic anemia highlights the negative impact of iron overload on morbidity/mortality. Eur J Haematol. 2007;78:487-94.

4. Neukirchen J, Fox F, Kündgen A, Nachtkamp K, Strupp C, Haas R, et al. Improved survival in MDS patients receiving iron chelation therapy - a matched pair analysis of 188 patients from the Düsseldorf MDS registry. Leuk Res. 2012;36:1067-70.

5. Rose C, Brechignac S, Vassilief D, Pascal L, Stamatoullas A, Guerci A, et al. ; GFM (Groupe Francophone des Myélodysplasies). Does iron chelation therapy improve survival in regularly transfused lower risk MDS patients? A multicenter study by the GFM (Groupe Francophone des Myélodysplasies). Leuk Res. 2010;34:864-70.

6. Lyons RM, Marek BJ, Paley C, Esposito J, Garbo L, DiBella N, et al. Comparison of 24-month outcomes in chelated and non-chelated lower-risk patients with myelodysplastic syndromes in a prospective registry. Leuk Res. 2014;38:149-54.

7. Gattermann N, Finelli C, Della Porta M, Fenaux P, Stadler M, Guerci-Bresler A, et al. Hematologic responses to deferasirox therapy in transfusion-dependent patients with myelodysplastic syndromes. Haematologica. 2012;97:1364-71.

8. Oliva EN, Ronco F, Marino A, Alati C, Praticò G, Nobile F. Iron chelation therapy associated with improvement of hematopoiesis in transfusion-dependent patients. Transfusion. 2010;50:1568-70.

9. Breccia M, Loglisci G, Salaroli A, Cannella L, Santopietro M, Alimena G. Deferasirox treatment interruption in a transfusion-requiring myelodysplastic patient led to loss of erythroid response. Acta Haematol. 2010;124:46-8.

10. Guariglia R, Martorelli MC, Villani O, Pietrantuono G, Mansueto G, D'Auria F, et al. Positive effects on hematopoiesis in patients with myelodysplastic syndrome receiving deferasirox as oral iron chelation therapy: a brief review. Leuk Res. 2011;35:566-70.

11. Fukushima T, Kawabata H, Nakamura T, Iwao H, Nakajima A, Miki M, et al. Iron chelation therapy with deferasirox induced complete remission in a patient with chemotherapy-resistant acute monocytic leukemia. Anticancer Res. 2011;31:1741-4.

12. Parsons DW, Jones S, Zhang X, Lin JC, Leary RJ, Angenendt P, et al. An integrated genomic analysis of human glioblastoma multiforme. Science. 2008;321:1807-12.

13. Yan H, Parsons DW, Jin G, McLendon R, Rasheed BA, Yuan W, et al. IDH1 and IDH2 mutations in gliomas. N Engl J Med. 2009;360:765-73.

14. Gross S, Cairns RA, Minden MD, Driggers EM, Bittinger MA, Jang HG, et al. Cancer-associated metabolite 2-hydroxyglutarate accumulates in acute myelogenous leukemia with isocitrate dehydrogenase 1 and 2 mutations. J Exp Med. 2010;207:339-44.

15. Ward PS, Patel J, Wise DR, Abdel-Wahab O, Bennett BD, Coller HA, et al. The common feature of leukemia-associated IDH1 and IDH2 mutations is a neomorphic enzyme activity converting alpha-ketoglutarate to 2-hydroxyglutarate. Cancer Cell. 2010;17:225-34.

16. Andersson AK, Miller DW, Lynch JA, Lemoff AS, Cai Z, Pounds SB, et al. IDH1 and IDH2 mutations in pediatric acute leukemia. Leukemia. 2011;25:1570-7.

17. Rakheja D, Medeiros LJ, Bevan S, Chen W. The emerging role of d-2-hydroxyglutarate as an oncometabolite in hematolymphoid and central nervous system neoplasms. Front Oncol. 2013;3:169.

18. Chotirat S, Thongnoppakhun W, Promsuwicha O, Boonthimat C, Auewarakul CU. Molecular alterations of isocitrate dehydrogenase 1 and 2 (IDH1 and IDH2) metabolic genes and additional genetic mutations in newly diagnosed acute myeloid leukemia patients. J Hematol Oncol. 2012;5:5.

19. Losman JA, Kaelin WG Jr. What a difference a hydroxyl makes: mutant IDH, (R)-2-hydroxyglutarate, and cancer. Genes Dev. 2013;27:836-52.

20. Murati A, Brecqueville M, Devillier R, Mozziconacci MJ, Gelsi-Boyer V, Birnbaum D. Myeloid malignancies: mutations, models and management. BMC Cancer. 2012;12:304.

21. Solary E, Bernard OA, Tefferi A, Fuks F, Vainchenker W. The Ten-Eleven Translocation-2 (TET2) gene in hematopoiesis and hematopoietic diseases. Leukemia. 2014;28:485-96.

22. Jin J, Hu C, Yu M, Chen F, Ye L, Yin X, et al. Prognostic value of isocitrate dehydrogenase mutations in myelodysplastic syndromes: a retrospective cohort study and meta-analysis. PLoS One. 2014;9:e100206.

23. Zhao X, Yang F, Li S, Liu M, Ying S, Jia X, et al. CpG island methylator phenotype of myelodysplastic syndrome identified through genome-wide profiling of DNA methylation and gene expression. Br J Haematol. 2014;165:649-58.

24. Yamazaki J, Issa JP. Epigenetic aspects of MDS and its molecular targeted therapy. Int J Hematol. 2013;97:175-82.

25. Issa JP. Epigenetic changes in the myelodysplastic syndrome. Hematol Oncol Clin North Am. 2010;24:317-30.

26. Shen L, Kantarjian H, Guo Y, Lin E, Shan J, Huang X, et al. DNA methylation predicts survival and response to therapy in patients with myelodysplastic syndromes. J Clin Oncol. 2010;28:605-13.

27. Calvo X, Nomdedeu M, Navarro A, Tejero R, Costa D, Muñoz C, et al. High levels of global DNA methylation are an independent adverse prognostic factor in a series of 90 patients with de novo myelodysplastic syndrome. Leuk Res. 2014;38:874-81.

28. Hirling H, Henderson BR, Kühn LC. Mutational analysis of the [4Fe-4S]-cluster converting iron regulatory factor from its RNA-binding form to cytoplasmic aconitase. EMBO J. 1994;13:453-61.

29. Kennedy MC, Emptage MH, Dreyer JL, Beinert H. The role of iron in the activation-inactivation of aconitase. J Biol Chem. 1983 ;258:11098-105.

30. Oexle H, Gnaiger E, Weiss G. Iron-dependent changes in cellular energy metabolism: influence on citric acid cycle and oxidative phosphorylation. Biochim Biophys Acta. 1999;1413:99-107.

31. Ito S, Ikuta K, Kato D, Lynda A, Shibusa K, Niizeki N et al. In vivo behavior of NTBI revealed by automated quantification system. Int J Hematol. 2016 in press

32. King A, Selak MA, Gottlieb E. Succinate dehydrogenase and fumarate hydratase: linking mitochondrial dysfunction and cancer. Oncogene. 2006;25:4675-82.

33. Selak MA, Armour SM, MacKenzie ED, Boulahbel H, Watson DG, Mansfield KD, et al. Succinate links TCA cycle dysfunction to oncogenesis by inhibiting HIF-alpha prolyl hydroxylase. Cancer Cell. 2005;7:77-85.

34. Cairns RA, Mak TW. Oncogenic isocitrate dehydrogenase mutations: mechanisms, models, and clinical opportunities. Cancer Discov. 2013;3:730-41.

35. Struys EA, Verhoeven NM, Ten Brink HJ, Wickenhagen WV, Gibson KM, Jakobs C. Kinetic characterization of human hydroxyacid-oxoacid transhydrogenase: relevance to D-2-hydroxyglutaric and gamma-hydroxybutyric acidurias. J Inherit Metab Dis. 2005;28:921-30.

36. Dang L, White DW, Gross S, Bennett BD, Bittinger MA, Driggers EM, et al. Cancer-associated IDH1 mutations produce 2-hydroxyglutarate. Nature. 2009;462:739-44.

37. Janin M, Mylonas E, Saada V, Micol JB, Renneville A, Quivoron C, et al. Serum 2-hydroxyglutarate production in IDH1- and IDH2-mutated de novo acute myeloid leukemia: a study by the Acute Leukemia French Association group. J Clin Oncol. 2014;32:297-305.

38. Fathi AT, Sadrzadeh H, Borger DR, Ballen KK, Amrein PC, Attar EC, et al. Prospective serial evaluation of 2-hydroxyglutarate, during treatment of newly diagnosed acute myeloid leukemia, to assess disease activity and therapeutic response. Blood. 2012;120:4649-52.

39. Pope WB, Prins RM, Albert Thomas M, Nagarajan R, Yen KE, Bittinger MA, et al. Non-invasive detection of 2-hydroxyglutarate and other metabolites in IDH1 mutant glioma patients using magnetic resonance spectroscopy. J Neurooncol. 2012;107:197-205.

40. Lazovic J, Soto H, Piccioni D, Lou JR, Li S, Mirsadraei L, et al. Detection of 2-hydroxyglutaric acid in vivo by proton magnetic resonance spectroscopy in U87 glioma cells overexpressing isocitrate dehydrogenase-1 mutation. Neuro Oncol. 2012;14:1465-72.

41. Navis AC, Niclou SP, Fack F, Stieber D, van Lith S, Verrijp K, et al. Increased mitochondrial activity in a novel IDH1-R132H mutant human oligodendroglioma xenograft model: in situ detection of 2-HG and α-KG. Acta Neuropathol Commun. 2013;1:18.

Figure legends

Figure 1: Accumulation of iron in bone marrow cells

A: Prussian blue staining of bone marrow smear samples. Blue dot staining was observed in the cytoplasm of iron overloaded bone marrow (Fe), which disappeared after iron chelation treatment (Fe + DFO). **B**: Intracellular iron levels of bone marrow analyzed by atomic absorption spectrometry. Intracellular iron levels were significantly higher in samples that were iron overloaded (Fe) than the control (Cont), and iron chelation (Fe + DFO) canceled this effect. $*P < 0.05$, n = 10

Figure 2: Comprehensive gene expression analysis by RNA sequencing

A: A volcano plot of gene expression analysis between the control (Cont) and iron overloaded (Fe) groups. **B:** A volcano plot of gene expression analysis between the Fe and iron chelated (Fe + DFO) groups. The red dotted line indicates the threshold fold change and *P*-value of the t-test. An absolute fold change number >1.5 and a *P*-value <0.05 were considered as differentially expressed genes. **C:** The numbers of gene extracted in each comparison (i.e., Cont. vs Fe and Fe vs Fe + DFO). There were 22 genes that overlapped both comparisons.

Figure 3: Gene expression analysis by digital PCR

The mRNA expression levels of *Aco1*, *Idh1*, *Pgm1*, and *Agl* in mice bone marrow of each group (control, Cont: circle; iron overloaded, Fe: square; and iron chelated, Fe + DFO: triangle) were analyzed by digital PCR analysis. Levels of *Aco1* (n = 20) and *Idh1* (n = 20) were significantly increased in the iron overloaded mice compared to the control group and decreased in the iron chelated mice compared to the iron overloaded mice. *Pgm1* (n = 8) was slightly increased in the iron overloaded mice than the control, but there was no significant change between the iron chelated and overloaded mice. *Agl* (n = 8) was significantly increased in the iron overloaded mice compared to control, but there was no significant change between the iron chelated and overloaded mice. $**P < 0.05$, $*P < 0.1$

Figure 4: Changes in the enzyme activity of ACO and IDH

Intracellular levels of ACO and IDH activities were measured by colorimetric enzyme activity assay. Both ACO (n = 10) and IDH (n = 10) activities of bone marrow cells were significantly

increased in the iron overloaded (Fe) mice than the control group (Cont) and decreased in the iron chelated (Fe + DFO) mice compared to iron overloaded mice. $*P < 0.05$

Figure 5: Changes in α-KG and 2-HG production

Whole organic acid was extracted from mice bone marrow samples and processed for GC-MS analysis. The total number of molecules per 109 cells was calculated based on the 2-HG standard data. Total intracellular α-KG and 2-HG levels were significantly increased in the iron overloaded (Fe) mice than the control group (Cont) and decreased in the iron chelated (Fe + DFO) mice compared to iron overloaded mice. $*P < 0.05$

Figure 6: DNA methylation enhanced by iron overload

Quantitative assay results for methylcytosine by fluorometric ELISA assay. DNA methylation in bone marrow (n = 10) was significantly increased in the iron overloaded (Fe) mice than the control (Cont) group and decreased in the iron chelated (Fe + DFO) mice than iron overloaded mice. $*P < 0.05$

Figure 7: Schematic representation of the pathways involved in increased DNA methylation and possible leukemogenesis via aberrant activity of glycogenolysis and the TCA cycle induced by iron overload.

Table

Function	Gene name
Enzymes associated with glucose metabolism	*Pgm1*
	Agl
	Idh1
	Idh3a
RNA polyadenilation enzyme	*Fip1l1*
DNA repairing protein	*Fancm*
Regulation of lipogenesis	*Mid1ip1*
Extracellular matrix glycoprotein	*Lamc1*
Intracellular protein transport	*Heatr5b*
Enzymes in the biosynthesis of coenzyme A	*Pank1*
Aminoacyl-tRNA synthetases	*Gars*

Regulator of cytokinesis	*Kif20b*
Golgi-derived retrograde transport vesicles with the ER	*Stx18*
RNA gene with undefined RNA class	*SNORD121A*
G-protein binding and guanyl-nucleotide exchange factor	*Ric8b*
ABL1 and/or ABL2 binding protein	*Abi2*
Member of the histone H4 family	*Hist1h4j*
RNA interference protein	*Ago4*
Protein sialylation	*St8sia4*
Transcription factor for maturation of T cell	*Hlx*
Endoplasmic reticulum transport	*Sytl1*
Cell cycle checkpoint control	*Rint1*

Yellow: up-regulated by iron and down-regulated by i
Green: down-regulated by iron and up-regulated by ii
RPKM, Reads per kilobase of exon model per million

Name of gene product	Cont. (means of RPKM)
Phosphoglucomutase 1	0.1003
Glycogen debranching enzyme	0.0121
Isocitrate dehydrogenase 1	0.0881
Isocitrate dehydrogenase 3a	0.1179
Factor Interacting With PAPOLA And CPSF1	0.0402
Fanconi Anemia, Complementation Group M	0.0303
MID1 Interacting Protein 1	0.0913
Laminin, Gamma 1	0.0411
HEAT Repeat Containing 5B	0.059
Pantothenate Kinase 1	0
Glycyl-TRNA Synthetase	0.197

Kinesin Family Member 20B	0.1457
Syntaxin 18	0
Small Nucleolar RNA, C/D Box 121A	0
RIC8 Guanine Nucleotide Exchange Factor B	0
Abl-Interactor 2	0
Histone Cluster 1, H4j	2.3926
Argonaute RISC Catalytic Component 4	0.524
ST8 □-N-Acetyl-Neuraminide □-2,8-Sialyltransferase 4	0.0417
H2.0-like homeobox protein	0.2525
synaptotagmin-like protein 1	0.2805
RAD50 Interactor 1	0.1351

ron chelation.
ron chelation.
ı mapped reads; FC, Fold change

Fe (means of RPKM)	DFO (means of RPKM)	FC (cont. vs Fe)
0.2013	0.1032	2.0075
0.0829	0.0315	6.8333
0.4217	0.103	4.7888
0.3353	0.0442	2.8435
0.0961	0.026	2.3924
0.1575	0.0521	5.2021
0.2612	0.1712	2.8595
0.1563	0.1031	3.8053
0.1419	0.0219	2.4063
0.1869	0	∞
0.419	0.0294	2.1267

0.2202	0.0126	1.5109
0.0904	0	∞
4.6787	0	∞
0.1235	0	∞
0.0657	0	∞
5.0486	1.9217	2.1101
0.0803	0.1409	-6.5222
0.0225	0.0895	-1.8539
0.1466	0.3329	-1.7222
0.0414	0.3023	-6.773
0.0223	0.1193	-6.0523

P value (cont. vs Fe)	FC (Fe vs DFO)	*P* value (Fe vs DFO)
0.004	-1.9508	0.0068
0.001	-2.6324	0.0328
0.035	-4.0934	0.0389
0.038	-7.5868	0.0234
0.048	-3.6883	0.0123
0.017	-3.0222	0.029
0.002	-1.5262	0.0078
0.009	-1.5154	0.0127
0.049	-6.4941	0.0335
0.0114	$-\infty$	0.0114
0.0195	-14.2368	0.0192

0.0369	-17.4127	0.0388
0.0464	-∞	0.0464
0.0464	-∞	0.0464
0.0464	-∞	0.0464
0.0464	-∞	0.0464
0.038	-2.6271	0.0132
0.022	1.7535	0.0009
0.041	3.9845	0.0138
0.046	2.2707	0.0399
0.02	7.2997	0.0039
0.019	5.3445	0.0349

Figure1

Click here to download Figure figure 1.tif

A

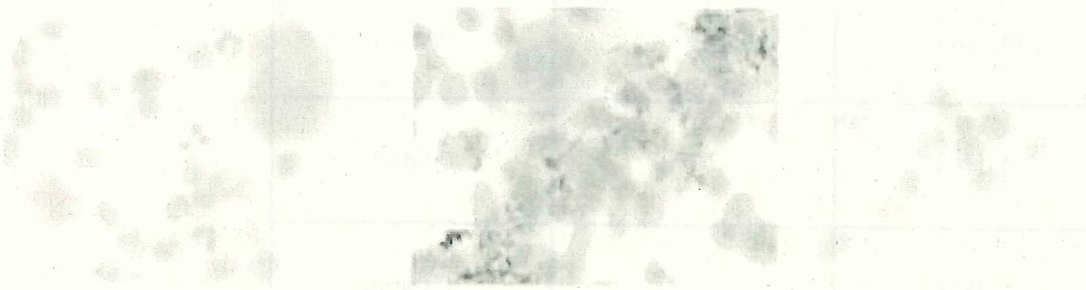

B

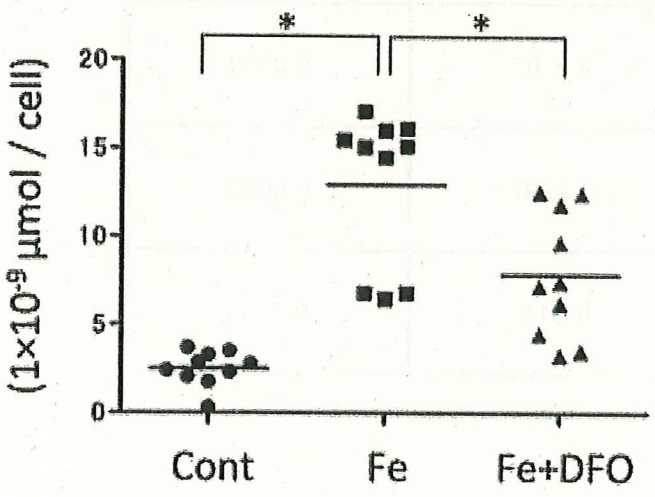

Figure2

Click here to download Figure figure 2-2.tif

Figure 2

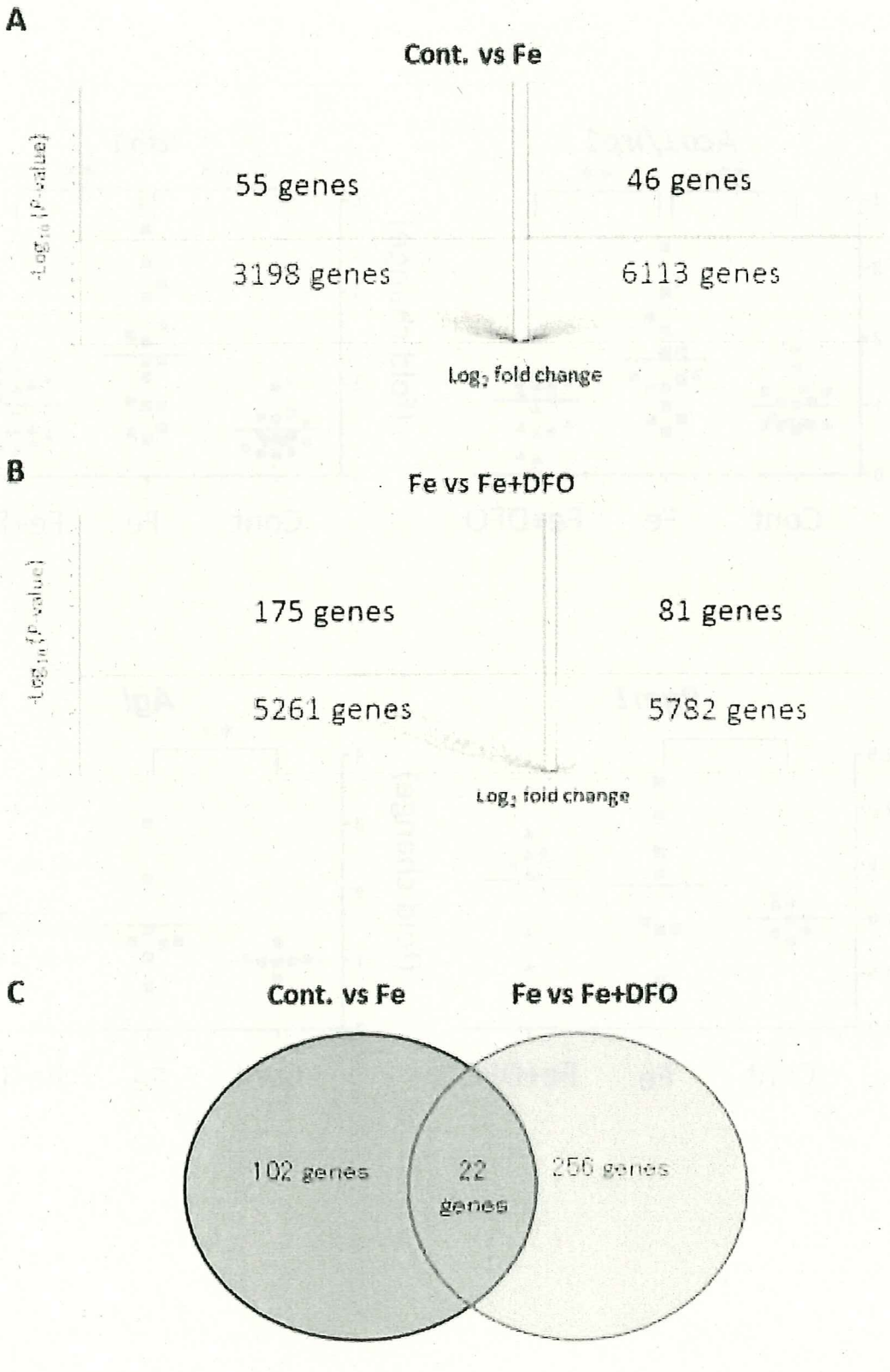

Figure3

Click here to download Figure figure 3.tif

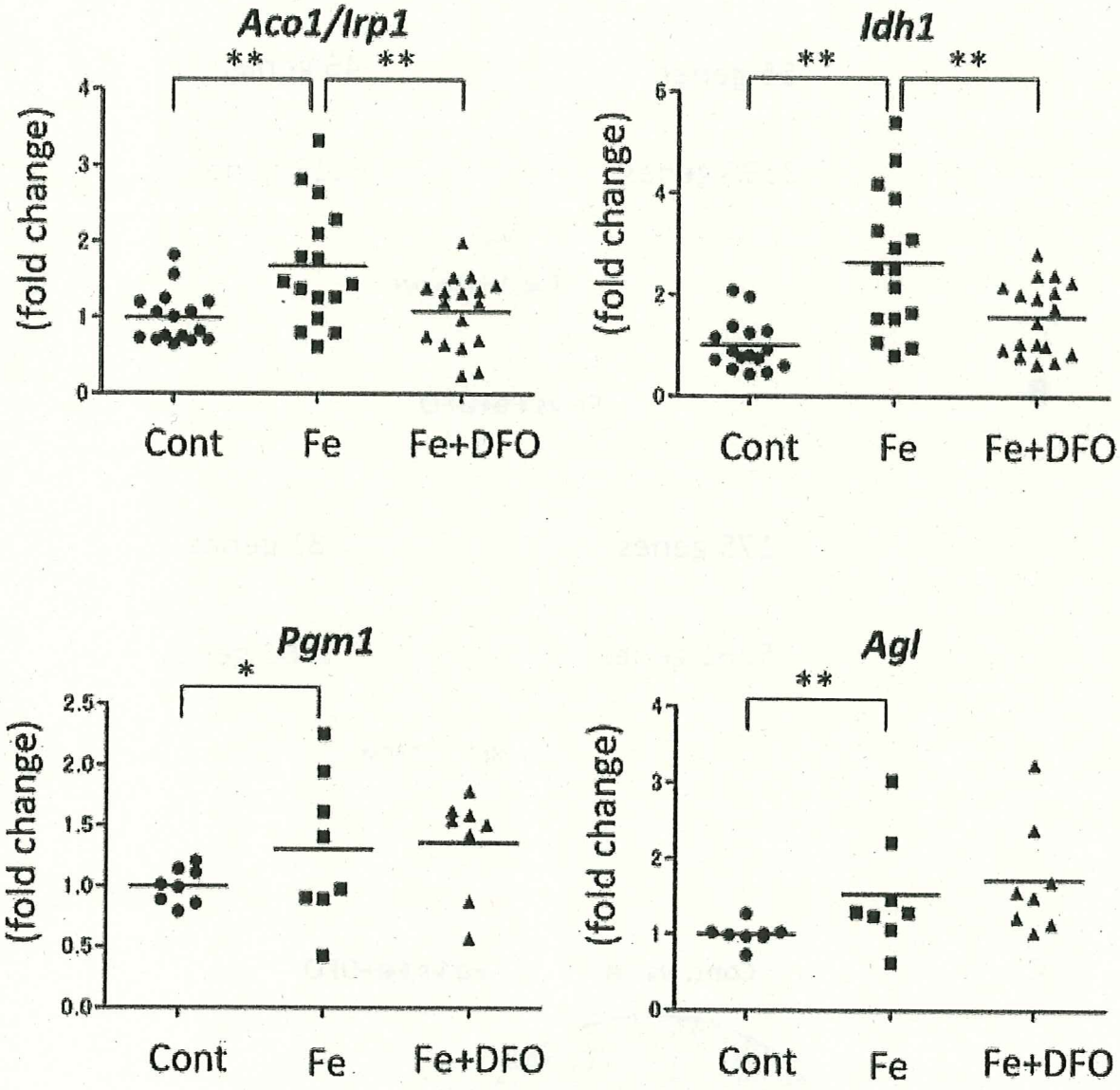

Figure4

Click here to download Figure figure 4.tif

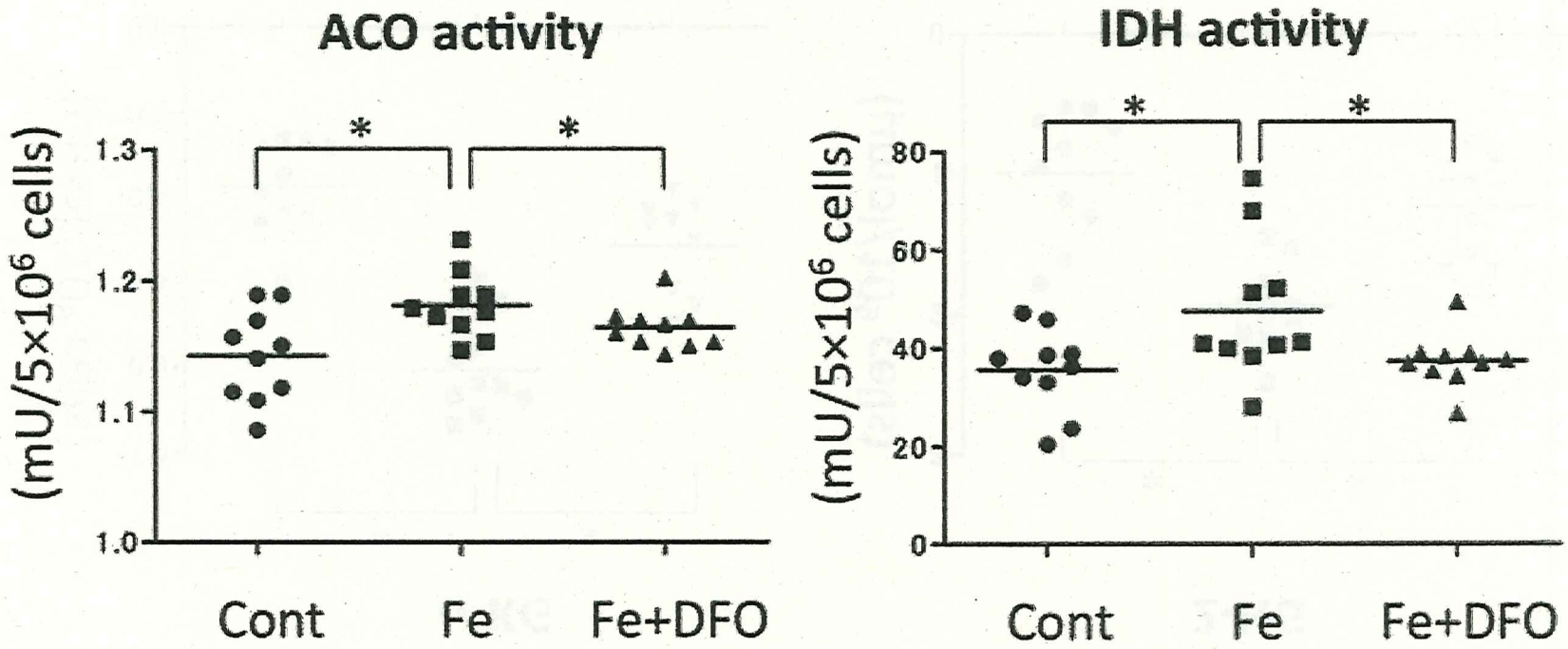

Figure5

Click here to download Figure figure 5.tif ±

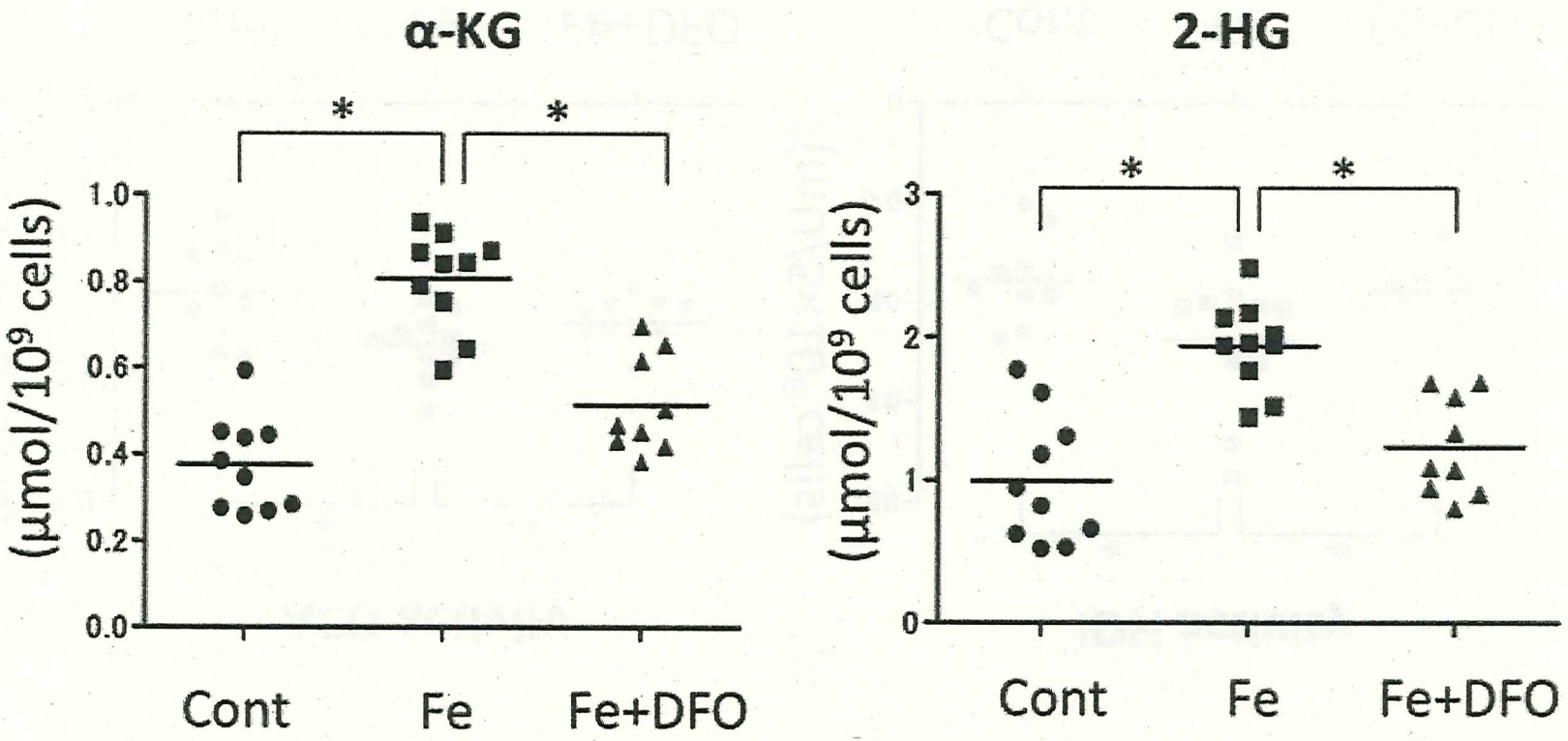

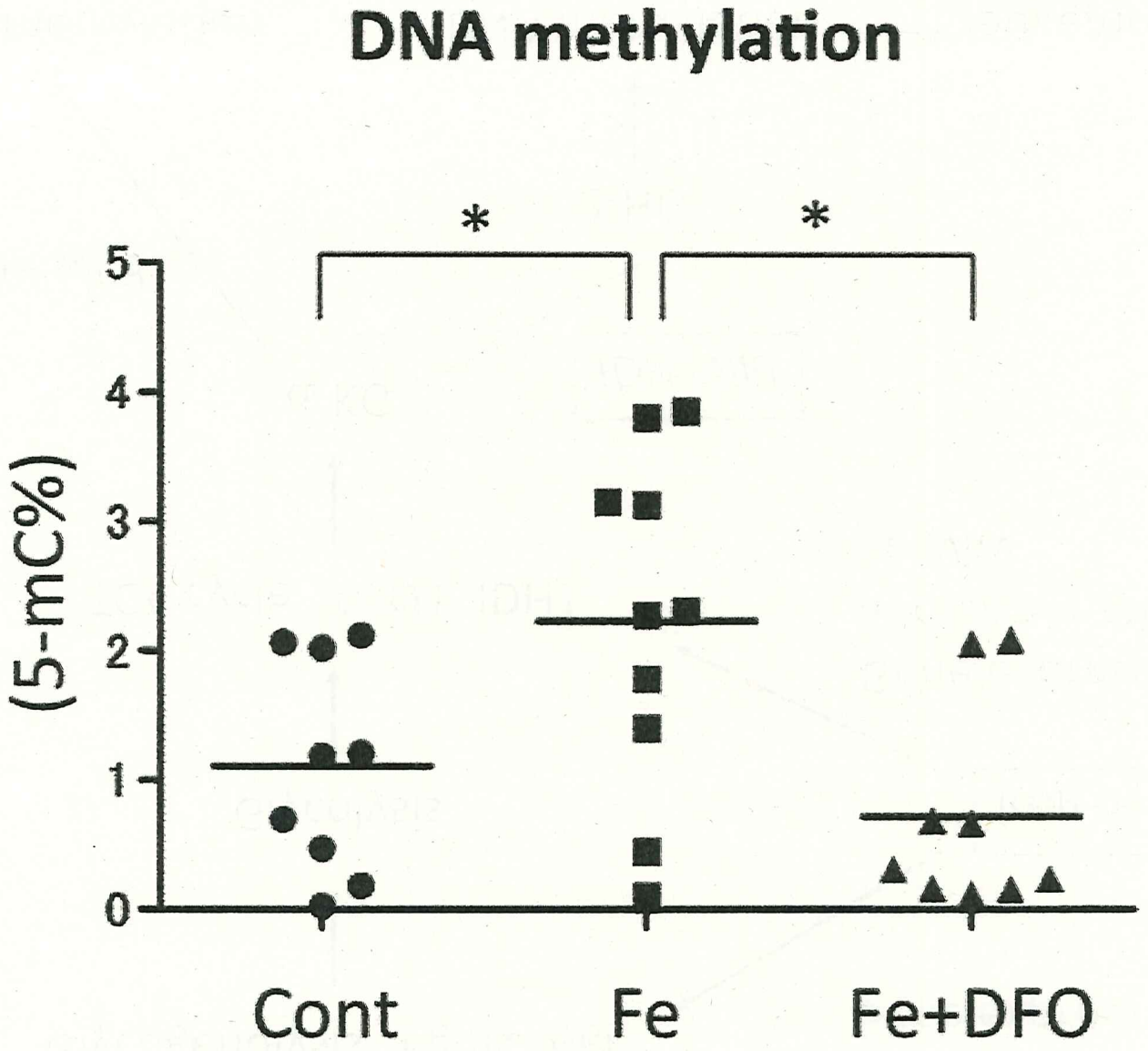

Figure7

Click here to download Figure figure 7.tif